Check for updates

Received: 11 September 2021 | Accepted: 14 December 2021

DOI: 10.1113/EP090052

Experimental Physiology WILEY

SHORT COMMUNICATION

Platelet-rich plasma affects gap junctional features in myofibroblasts in vitro via vascular endothelial growth factor (VEGF)-A/VEGF receptor

Chiara Sassoli[1] | Rachele Garella[2] | Flaminia Chellini[1] | Alessia Tani[1] | Paola Pavan[3] | Franco Bambi[3] | Sandra Zecchi-Orlandini[1] | Roberta Squecco[2]

[1] Section of Anatomy and Histology, Department of Experimental and Clinical Medicine, University of Florence, Florence, Italy

[2] Section of Physiological Sciences, Department of Experimental and Clinical Medicine, University of Florence, Florence, Italy

[3] Transfusion Medicine and Cell Therapy Unit, 'A. Meyer' University Children's Hospital, Florence, Italy

Correspondence
Roberta Squecco, Department of Experimental and Clinical Medicine, Section of Physiological Sciences, University of Florence, Viale Morgagni 63, 50134 Florence, Italy.
Email: roberta.squecco@unifi.it

Funding information
MIUR (Ministry of Education, University and Research, Italy); Ministero dell'Istruzione, dell'Università e della Ricerca, Grant/Award Number: FFABR-MIUR 2017

Edited by: Jason Peart

Abstract

Despite increasing experimental evidence, the antifibrotic potential of platelet-rich plasma (PRP) remains controversial, and its mechanisms of action are not fully clarified. This short report extends our previous research on the capability of PRP to prevent the in vitro differentiation of fibroblasts toward myofibroblasts, the key effectors of fibrosis, induced by the profibrotic agent transforming growth factor-β1 (TGF-β1). In particular, we focused on the involvement of signalling mediated by vascular endothelial growth factor (VEGF)-A/VEGF receptor (VEGFR) in the PRP-induced fibroblast response, highlighting gap junction features. Electrophysiological and morphological analyses revealed that PRP hindered morphofunctional differentiation of both murine NIH/3T3 and human primary adult skin fibroblasts toward myofibroblasts as judged by the analysis of membrane phenomena, α-smooth muscle actin and vinculin expression and cell morphology. Neutralization of VEGF-A by blocking antibodies or pharmacological inhibition of VEGFR by KRN633 in TGF-β1-treated fibroblasts prevented the PRP-promoted effects, such as the reduction of voltage-dependent transjunctional currents in cell pairs and a decreased expression of connexin 43, the typical connexin isoform forming voltage-dependent connexons. The role of VEGF-A in inhibiting these events was confirmed by treating TGF-β1-stimulated fibroblasts with soluble VEGF-A. The results obtained when cells were differentiated using KRN633 alone suggest an antagonistic cross-talk between TGF-β1 and VEGFR. In conclusion, this study identifies, for the first time, gap junction currents as crucial targets in the VEGF-A/VEGFR-mediated antifibrotic pathway and provides new insights into mechanisms behind the action of PRP in preventing differentiation of fibroblasts to myofibroblasts.

KEYWORDS
connexin 43, fibrosis, gap junctions, myofibroblasts, platelet-rich plasma, vascular endothelial growth factor

© 2021 The Authors. Experimental Physiology © 2021 The Physiological Society

1 | INTRODUCTION

Fibrosis is a complex disease affecting multiple organs that can lead to serious alterations of their functionality. Development of an effective antifibrotic treatment is thus mandatory (Miao et al., 2021; Sassoli et al., 2021). Increasing evidence supports the antifibrotic potential of platelet-rich plasma (PRP) (Moghadam et al., 2017; Shoeib et al., 2018; Vu et al., 2015), a plasma preparation with a platelet concentration $> 2.0 \times 10^6$ cells/μL, representing a storage vehicle of several bioactive molecules (Chellini et al., 2019). However, the effects of PRP are still controversial and the mechanisms underpinning its action are not fully clarified, calling into question its clinical application for antifibrotic purposes (Guillodo et al., 2016; Lynch & Bashir, 2016; Schroeder et al., 2016).

We previously demonstrated that PRP prevents the in vitro differentiation of fibroblasts to myofibroblasts by counteracting the canonical profibrotic transforming growth factor-β1 (TGF-β1)/Smad3 signalling (Chellini et al., 2018; Squecco et al., 2020). Myofibroblasts are regarded as the key effectors in fibrosis, showing features of both collagen-synthesizing fibroblasts and contractile cells, exhibiting transmembrane ion currents similar to those found in excitable cells and well-assembled myofilament bundles containing α-smooth muscle actin (α-sma) (Pakshir et al., 2020; Squecco et al., 2015). Platelet-rich plasma was demonstrated to be able to: (1) reduce the increase of TGF-β1-induced α-sma expression, through vascular endothelial growth factor (VEGF)-A/VEGF receptor (R) 1-mediated signalling (Chellini et al., 2018); and (2) abolish the occurrence of TGF-β1-induced voltage-dependent gap junction (GJ) currents while inhibiting the expression of connexin 43 (Cx43), a ubiquitous connexin (Cx) isoform forming voltage-dependent connexons, during the myofibroblast differentiation (Squecco et al., 2020). The GJs and the related Cxs, especially Cx43, play essential roles to coordinate profibrotic signalling in different tissues, including renal (Xu et al., 2021) and cardiac (Nagaraju et al., 2019) tissues.

By electrophysiological and morphological analyses, the aim of this in vitro study was to evaluate the involvement of VEGF-A/VEGFR in the PRP-induced responses of murine NIH/3T3 and human primary skin fibroblasts undergoing myo-differentiation, in terms of GJ currents and Cx43 expression, extending our previous research on this topic.

New Findings

- **What is the central question of this study?**
  It is a challenge to discover effective therapies for fibrosis. Increasing evidence supports the antifibrotic potential of platelet-rich plasma (PRP) as a source of bioactive molecules, such as vascular endothelial growth factor (VEGF)-A. However, the effects and mechanisms of action of PRP need to be clarified.
- **What is the main finding and its importance?**
  This report clarifies the mechanisms mediating the antifibrotic action of PRP, strengthening the role of VEGF-A/VEGF receptor, and identifies gap junction currents and connexin 43 as novel targets of this pathway in the fibroblast-to-myofibroblast transition induced by the transforming growth factor-β1.

2 | METHODS

2.1 | Ethical approval

The specimens from humans were collected according to the standards set by the latest version of the *Declaration of Helsinki*. All subjects provided written informed consent. For the present experimentation, thawed PRP aliquots previously prepared and stored at −80°C were used (Chellini et al., 2018). The PRP was obtained from the whole blood of adult healthy voluntary donors, and the procedures were regulated by the National legislation DM 2-11-2015/GU n 300 (28.12.15/19A05957). Human primary adult skin fibroblasts were isolated and cultured as reported in the study by Romano et al. (2020). Skin samples were collected as waste material from plastic surgeries of six healthy subjects at the Plastic and Reconstructive Microsurgery Center, Careggi University Hospital, Florence, Italy. The study was approved by the local ethics committee (Comitato Etico Regionale per la Sperimentazione Clinica della Toscana—sezione AREA VASTA CENTRO, Florence, Italy; approval number 16687_bio; approval date 14 April 2020).

2.2 | Platelet-rich plasma

We tested thawed ready-to-use activated leucocyte-free PRP aliquots (final platelet concentration 2×10^6 platelets/μL; platelet activation induced by a 10% calcium digluconate solution) from blood of healthy adult donors subjected to plasma-platelet apheresis (Haemonetics MCS; Haemonetics, Milan, Italy), previously prepared and stored at −80°C (Chellini et al., 2018). In brief, after the collection, platelet units were stored in a shaker incubator, and the plasma units were immediately frozen at −80°C. Subsequently, plasma units were thawed at 4°C for 16 h to obtain the cryoprecipitate by syphoning. Then, platelets were resuspended in the cryoprecipitate and adjusted to the final concentration.

2.3 | Cell culture and treatments

The experimentation was carried out on murine NIH/3T3 fibroblasts and on human primary adult skin fibroblasts. NIH/3T3 fibroblasts are the same cell model used in our previous studies on this topic (Chellini et al., 2018; Squecco et al., 2020), whose capability to respond to TGF-β1 stimulation is similar to that of human dermal and primary

1469445x, 2022, 2, Downloaded from https://physoc.onlinelibrary.wiley.com/doi/10.1113/EP090052 by Universita Di Firenze Sistema, Wiley Online Library on [06/08/2024]. See the Terms and Conditions (https://onlinelibrary.wiley.com/terms-and-conditions) on Wiley Online Library for rules of use; OA articles are governed by the applicable Creative Commons License

cardiac fibroblasts, as previously established (Chellini et al., 2018; Squecco et al., 2015).

Murine NIH/3T3 fibroblasts [American Type Culture Collection, Manassas, VA, USA; catalogue number (Cat#) CRL-1658, Research Resource Identifiers (RRID): CVCL_0594] were grown in proliferation medium [PM; Dulbecco's modified Eagle's medium (DMEM) supplemented with 4.5 g/L glucose, 10% fetal bovine serum (FBS) and 1% penicillin/streptomycin; Sigma, Milan, Italy], at 37°C in a humidified atmosphere of air enriched with 5% CO_2. Human primary fibroblasts were kindly provided by Professor Mirko Manetti. Cells were expanded in PM composed of DMEM supplemented with 15% FBS, 2 mM L-glutamine (CAT# BE17-605E/U1; Lonza, Basel, Switzerland), 100 U/mL of penicillin and 100 U/mL of streptomycin (Romano et al., 2020). Differentiation to myofibroblasts was induced by culturing fibroblasts in a differentiation medium, DM (DMEM, 2% FBS and 2 ng/mL of TGF-β1; PeproTech, Rocky Hill, NJ, USA, Cat# 100-21-10UG, Lot# 0716209-1) for 48 h. Platelet-rich plasma was added to DM at the dilution of 1:50 (Squecco et al., 2020). In parallel, cells were cultured: (1) in DM plus a specific ATP-competitive inhibitor of VEGFR tyrosine kinase activity, KRN633 (Santa Cruz Biotechnology, Santa Cruz, CA, USA; IC_{50} = 170 nM, Cat# sc-204379, Lot# B1810, dilution in DMSO, Sigma, Cat# 472301) in the absence or presence of PRP; (2) in DM in the presence of PRP plus mouse monoclonal anti-VEGF-A neutralizing antibodies (10 μg/mL; Sigma, Cat# V4758, Lot# 066K1428, RRID:AB_477621). Specificity of blocking antibodies was verified by using irrelevant isotype-matched IgG (Chellini et al., 2018). Cells cultured in DMSO (1:1,000) were used as the internal control for KRN633 treatment. In parallel experiments, cells were cultured in DM in the presence of soluble VEGF-A (2 and 20 ng/mL; Sigma; Cat# 4512-5UG, Lot# 091M1209V) based on our previous studies (Chellini et al., 2018; Sassoli et al., 2012).

2.4 | Electrophysiological records

Recordings were performed using the dual whole-cell patch-clamp technique at 22°C as described by Squecco et al. (2020). The experimental apparatus comprised an Axopatch 200B amplifier, an analog-to-digital/digital-to-analog interface (Digidata 1200) and pCLAMP 6 software (Axon Instruments, Union City, CA, USA). The resting membrane potential (RMP) was measured in current-clamp mode (stimulus: I = 0 pA). Currents flowing through GJs of a cell pair (transjunctional current, I_j) were evoked in voltage-clamp mode from a holding potential (HP) of 0 mV, using a bipolar 5 s pulse protocol with transjunctional voltages, V_j, ranging from ±10 to ±150 mV, in 20 mV increments. The value of I_j was normalized for cell capacitance for proper comparison. Specifically, instantaneous I_j ($I_{j,inst}$) represents the current peak amplitude, and steady-state I_j ($I_{j,ss}$) the amplitude measured at the end of each pulse. Related conductances (G_j) were calculated by the ratios: $G_{j,inst} = I_{j,inst}/V_j$ and $G_{j,ss} = I_{j,ss}/V_j$.

2.5 | Confocal laser scanning microscopy

Indirect immunofluorescence was performed on fixed cells (Squecco et al., 2020). Primary antibodies (overnight, 4°C): mouse monoclonal anti-α-sma (1:100; Abcam, Cambridge, UK, Cat# ab7817, Lot# GR3246513, RRID: AB_262054), mouse monoclonal hVIN-1 anti-vinculin (1:100; Sigma, Cat# V9131, Lot# 036M4797V, RRID: AB_477629) and rabbit polyclonal anti-Cx43 (1:100; Cell Signaling Technology Danvers, MA, USA, Cat# 3512S, Lot# 7, RRID: AB_2294590). Secondary antibodies [1 h, room temperature (RT)]: goat anti-mouse Alexa Fluor 488-conjugated IgG (1:200; Molecular Probes-Thermo Fisher Scientific, Eugene, OR, USA, Cat# A11001, Lot# 1752514, RRID: AB_2534069), goat anti-rabbit Alexa Fluor 488-conjugated IgG (1:200; Molecular Probes, Cat# A11034, Lot# 1851447, RRID: AB_2576217) and goat anti-mouse Cy5-conjugated IgG (1:200; Chemicon, Temecula, CA, USA, Cat# AP127S, Lot# 21040798). Nuclei were counterstained with propidium iodide (1:30; 10 s at RT; Molecular Probes, Cat# P3566, Lot# 506444). Observations were performed under a confocal Leica TCS SP5 microscope (Leica Microsystems, Mannheim, Germany) by using a Leica Plan Apo 63×/1.43 NA oil-immersion objective. Optical section series (1,024 × 1,024 pixels each, pixel size 204.3 nm, 209 μm × 209 μm optical square field, 0.4 μm in thickness) were acquired at intervals of 0.6 μm and projected onto a single 'extended focus' image.

2.6 | Statistical analysis

Densitometric analyses of α-sma, vinculin and Cx43 fluorescent signal intensity were performed on digitized images using IMAGEJ (RRID: SCR_003070) in five regions of interest (ROI; 50 μm × 50 μm) for each confocal stack (two for each experimental point performed in duplicate). The experiments were performed in triplicate (n for each experimental point = ROI = 60). Morphometric analysis of the mean cell surface area was performed on digitized differential interference contrast (DIC) images at the same magnification, using IMAGEJ (Chellini et al., 2020). Three cells per image (two images for each experimental point performed in duplicate) were analysed. The experiments were performed in triplicate (n = cells = 36). One-way ANOVA with Tukey's post hoc test was used for multiple comparisons, performed with the open-source statistical software JAMOVI v.2.2.2 (https://www.jamovi.org).

Electrophysiological data were collected from a typical, randomly chosen group from total cell populations (n = cells). Student's unpaired t-test was used to compare two data sets. One-way ANOVA with Bonferroni's post hoc correction was used for multiple comparisons. MICROSOFT EXCEL (Microsoft, Washington, USA, RRID: SCR_016137) was used to carry out statistical analysis. Values are reported as the mean ± SD. A value of $P \leq 0.05$ was considered statistically significant. MICROSOFT EXCEL was used to create graphs.

1469445x, 2022, 2, Downloaded from https://physoc.onlinelibrary.wiley.com/doi/10.1113/EP090052 by Universita Di Firenze Sistema, Wiley Online Library on [06/08/2024]. See the Terms and Conditions (https://onlinelibrary.wiley.com/terms-and-conditions) on Wiley Online Library for rules of use; OA articles are governed by the applicable Creative Commons License

3 | RESULTS

The successful acquisition of the myofibroblastic phenotype by NIH/3T3 fibroblasts cultured in DM was assessed by RMP analysis (Figure 1a,b; Table A1) and by morphological and immunocytochemical characterization (Figure 1c–p; Tables A2–A4). Although NIH/3T3 myofibroblasts in DM tended to have a more depolarized RMP value (−41.4 ± 7.5 mV; $n = 5$) compared with undifferentiated fibroblasts in PM (−62.2 ± 18.8 mV; $n = 5$), the differences were not statistically significant (Figure 1b; $P = 0.059$). However, myofibroblasts showed higher α-sma and vinculin expression ($n = 60$ ROI, $P < 0.0001$ for both markers; Figure 1c,d,n,o; Tables A2 and A3). The α-sma appeared well organized, conceivably along stress fibre-like structures mostly arranged in a parallel manner across the cytoplasm and attached to vinculin-enriched aggregates. These cells appeared larger, with a more polygonal shape and a greater surface area in comparison to undifferentiated cells, which were smaller and more spindle shaped (Figure 1c,d,p; $n = 36$, $P < 0.0001$; Table A4).

Although NIH/3T3 cells cultured in DM+PRP showed a more repolarized RMP (−50.2 ± 23.75 mV; $n = 5$) compared with those in DM, the differences were not statistically significant (Figure 1b; $P = 0.46$). However, these cells showed a significantly reduced expression of α-sma and vinculin ($n = 60$ ROI, $P < 0.0001$ for both markers) at focal adhesion sites and a morphology more similar to that of undifferentiated cells ($n = 36$ cells, $P < 0.0001$; Figure 1e,n–p).

The same cellular response to TGF-β1 and the capability of PRP to counteract the TGF-β1-induced myofibroblast differentiation was confirmed on primary human skin fibroblasts (Figure 2). When evaluated in these cells, the RMP was significantly depolarized in myofibroblasts cultured in DM (−49.4± 3.2 mV; $n = 5$) compared with their control counterparts cultured in PM (−58.0 ± 1.4 mV, $n = 5$; $P = 0.002$; Figure 2a,b; Table A5). Similar to the murine fibroblasts, the RMP recorded from human fibroblasts in DM+PRP was not significantly repolarized (−52.2 ± 5.17 mV; $n = 7$) compared with that recorded in DM ($P = 0.276$, Figure 2b); however, they appeared clearly spindle shaped and exhibited a reduction of α-sma expression, in comparison to that of differentiating cells (Figure 2c,e,g). These observations suggest the ability of PRP to hinder differentiation in both fibroblastic cell populations.

The role of VEGF-A/VEGFR in mediating the fibroblast response to PRP was assessed by culturing cells in DM+PRP either with KRN633, a selective pharmacological VEGFR inhibitor, (DM+PRP+KRN633) or with anti-VEGF-A neutralizing antibodies (DM+PRP+AntiVEGF-A Ab). Cells cultured in DM+PRP+DMSO and cells cultured in DM+PRP in the presence of irrelevant isotype-matched IgG (DM+PRP+IgG) were used as internal controls for cells in DM+PRP+KRN633 and cells in DM+PRP+AntiVEGF-A Ab, respectively.

Regarding the RMP, in differentiating NIH/3T3 cells the effect of PRP was scarcely altered by the presence of these hindering agents, and kept on showing the tendency to repolarize the membrane, although we did not find statistically significant differences in RMP values from cells cultured in DM+PRP+KRN633 ($n = 6$) compared with DM+PRP+DMSO ($n = 4$) ($P = 0.372$; DM+PRP+DMSO vs. DM+PRP, $n = 5$, $P = 0.967$; DM+PRP+KRN633 vs. DM+PRP, $P = 0.472$) or from cells in DM+PRP+AntiVEGF-A Ab ($n = 6$) compared with DM+PRP+IgG ($n = 5$) ($P = 0.226$; DM+PRP+IgG vs. DM+PRP, $P = 0.859$; DM+PRP+AntiVEGF-A Ab vs. DM+PRP, $P = 0.586$) (Figure 1b).

In contrast, KRN633 or VEGF-A Ab abrogated the effects of PRP, preventing the downregulation of α-sma and vinculin expression ($n = 60$ ROI, DM+PRP+KRN633 vs. DM+PRP+DMSO and DM+PRP+AntiVEGF-A vs. DM+PRP+IgG, $P < 0.0001$ for both markers; DM+PRP+DMSO vs. DM+PRP, $P = 1$; DM+PRP+KRN633 vs. DM+PRP, $P < 0.0001$ for both markers; DM+PRP+IgG vs. DM+PRP, α-sma $P = 0.983$, vinculin $P = 0.789$; DM+PRP+AntiVEGF vs. DM+PRP $P < 0.0001$ for both markers) and the reduction in cell surface area ($n = 36$, DM+PRP+KRN633 vs. DM+PRP+DMSO and DM+PRP+AntiVEGF-A vs. DM+PRP+IgG, $P < 0.0001$; DM+PRP+DMSO vs. DM+PRP, $P = 1$; DM+PRP+IgG vs. DM+PRP, $P = 0.071$ DM+PRP+KRN633 vs. DM+PRP and DM+PRP+AntiVEGF vs. DM+PRP, $P < 0.0001$) (Figure 1e,g,i,j,k,n–p).

In particular, NIH/3T3 cells in DM+PRP+KRN633 showed morphological features comparable to those of cells in DM (Figure 1d,i,n,o; $n = 60$ ROI, α-sma $P = 1$; vinculin $P = 0.701$; cell surface area, $n = 36$, $P = 0.926$). In contrast, NIH/3T3 cells in DM+PRP+AntiVEGF-A Ab showed lower α-sma and vinculin expression compared with cells in DM (Figure 1d,k,n,o; $n = 60$ ROI, α-sma, $n = 60$, $P = 0.007$; vinculin, $n = 60$, $P = 0.049$) but a similar cell surface area (Figure 1d,k,p; $n = 36$, $P = 0.95$).

Furthermore, in order to evaluate potential cross-talk between TGF-β1 signalling and VEGFR, cells were cultured in DM+KRN633 alone. NIH/3T3 cells in DM+DMSO, as an internal control, showed electrophysiological and morphological features similar to those in DM (Figure 1b, RMP, DM+DMSO, $n = 4$, vs. DM, $n = 5$, $P = 0.655$; Figure 1d,f,n–p, α-sma and vinculin, $n = 60$ ROI, $P = 1$; cell surface area, $n = 36$, $P = 1$). The RMP values from cells in DM+KRN633 were depolarized (−42.4 ± 2.8 mV; $n = 8$), like those recorded in DM+DMSO ($n = 4$, $P = 0.788$). Likewise, the morphological analysis revealed the acquisition of a typical myofibroblastic phenotype (Figure 1f,h,n–p; DM+KRN633 vs. DM+DMSO or vs. DM α-sma and vinculin, $n = 60$ ROI, $P = 1$; cell surface area, $n = 36$, $P = 1$).

To confirm the involvement of VEGF-A in affecting TGF-β1-promoted generation of myofibroblasts, NIH/3T3 fibroblasts were cultured in DM plus soluble VEGF-A at two concentrations, 2 and 20 ng/mL (DM+VEGF-A 2 and DM+VEGF-A 20). In both cases, cells showed RMP values comparable to DM+PRP (Figure 1b; for VEGF-A 2, $n = 5$, $P = 0.802$; and for VEGF-A 20, $n = 4$, $P = 0.692$). In particular, DM+VEGF-A 20 significantly repolarized the membrane compared with DM ($P = 0.007$). Both VEGF-A concentrations caused a marked decrease of α-sma and vinculin expression in comparison to DM ($n = 60$ ROI, $P < 0.0001$ for both markers) and prevented morphological modifications ($n = 36$, $P < 0.0001$) induced by DM itself (Figure 1l–p). Noteably, DM+VEGF-A 20 elicited a more marked reduction of α-sma expression than DM+VEGF-A 2 ($n = 60$ ROI, $P = 0.033$); however,

1469445x, 2022, 2, Downloaded from https://physoc.onlinelibrary.wiley.com/doi/10.1113/EP090052 by Universita Di Firenze Sistema, Wiley Online Library on [06/08/2024]. See the Terms and Conditions (https://onlinelibrary.wiley.com/terms-and-conditions) on Wiley Online Library for rules of use; OA articles are governed by the applicable Creative Commons License

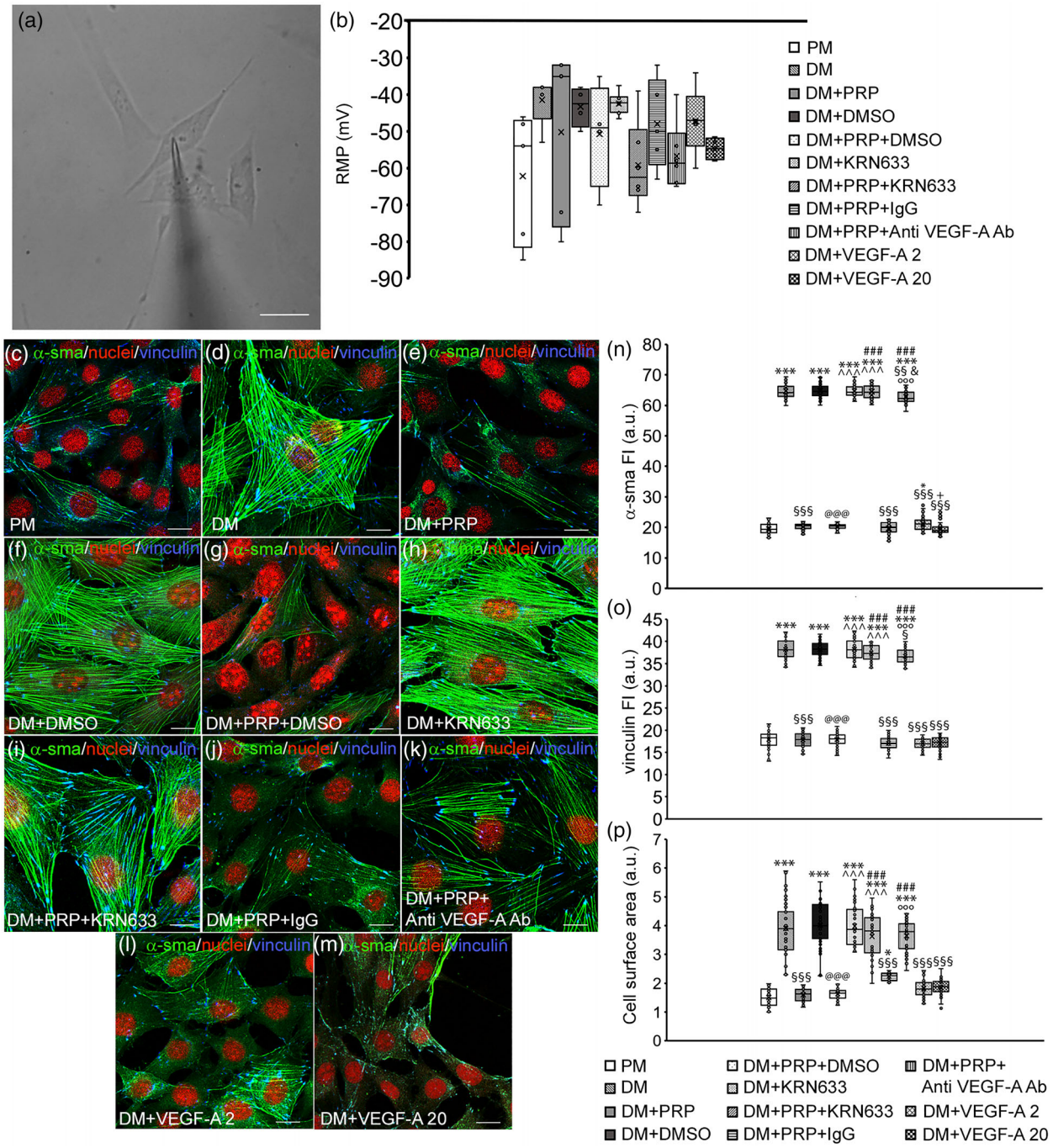

FIGURE 1 Morphofunctional evaluation of NIH/3T3 fibroblast-to-myofibroblast transition. (a) Typical fibroblast (in PM, proliferation medium) impaled by the patch electrode (scale bar represents 20 μm). (b) Resting membrane potential (RMP, in millivolts; $n = 4–8$ cells; one-way ANOVA with Bonferroni's correction, $P = 0.074$, d.f. = 56). Exact P-values of any comparison are reported in Table A1 for clarity. (c–m) Representative immunofluorescence analysis of α-smooth muscle actin (α-sma) and vinculin expression. Nuclei are counterstained with propidium iodide. Scale bars represent 10 μm. (n,o) Densitometric analysis of the fluorescence intensity (FI, in arbitrary units, a.u) of indicated markers. (p) Morphometric analysis of mean cell surface area. Abbreviations: Anti VEGF-A (vascular endothelial growth factor-A) Ab, anti-VEGF-A neutralizing antibodies; DM, differentiation medium; IgG, irrelevant isotype-matched IgG; KRN633, selective pharmacological VEGFR inhibitor; PM, proliferation medium; PRP, platelet-rich plasma; VEGF-A 2, 20, soluble VEGF-A 2 or 20 ng/mL. Values are the mean ± SD. Significance of differences in (n) (α-sma): *** versus PM ($P < 0.0001$); * versus PM ($P = 0.05$); §§§ versus DM ($P < 0.0001$); §§ versus DM ($P = 0.007$); $^{###}$ versus DM+PRP ($P < 0.0001$); $^{@@@}$ versus DM+DMSO ($P < 0.0001$); $^{\wedge\wedge\wedge}$ versus DM+PRP+DMSO ($P < 0.0001$); $^{\&}$ versus DM+PRP+KRN ($P = 0.019$); $^{°°°}$ versus DM+PRP+IgG ($P < 0.0001$); $^{+}$ versus VEGF-A 2 ($P = 0.033$). Significance of differences in (o) (vinculin): *** versus PM ($P < 0.0001$); §§§ versus DM ($P < 0.0001$); § versus DM ($P = 0.049$); $^{###}$ versus DM+PRP ($P < 0.0001$); $^{@@@}$ versus DM+DMSO ($P < 0.0001$); $^{\wedge\wedge\wedge}$ versus DM+PRP+DMSO ($P < 0.0001$); $^{°°°}$ versus DM+PRP+IgG ($P < 0.0001$). In (n) and (o), one-way ANOVA with Tukey's post hoc test, $n = 60$ regions of interest. Significance of differences in (p) (cell surface area, one-way ANOVA with Tukey's post hoc test, $n = 36$ cells): *** versus PM ($P < 0.0001$); * versus PM ($P = 0.026$); §§§ versus DM ($P < 0.0001$); $^{###}$ versus DM+PRP ($P < 0.0001$); $^{@@@}$ versus DM+DMSO ($P < 0.0001$); $^{\wedge\wedge\wedge}$ versus DM+PRP+DMSO ($P < 0.0001$); $^{°°°}$ versus DM+PRP+IgG ($P < 0.0001$)

1469445x, 2022, 2, Downloaded from https://physoc.onlinelibrary.wiley.com/doi/10.1113/EP090052 by Universita Di Firenze Sistema, Wiley Online Library on [06/08/2024]. See the Terms and Conditions (https://onlinelibrary.wiley.com/terms-and-conditions) on Wiley Online Library for rules of use; OA articles are governed by the applicable Creative Commons License

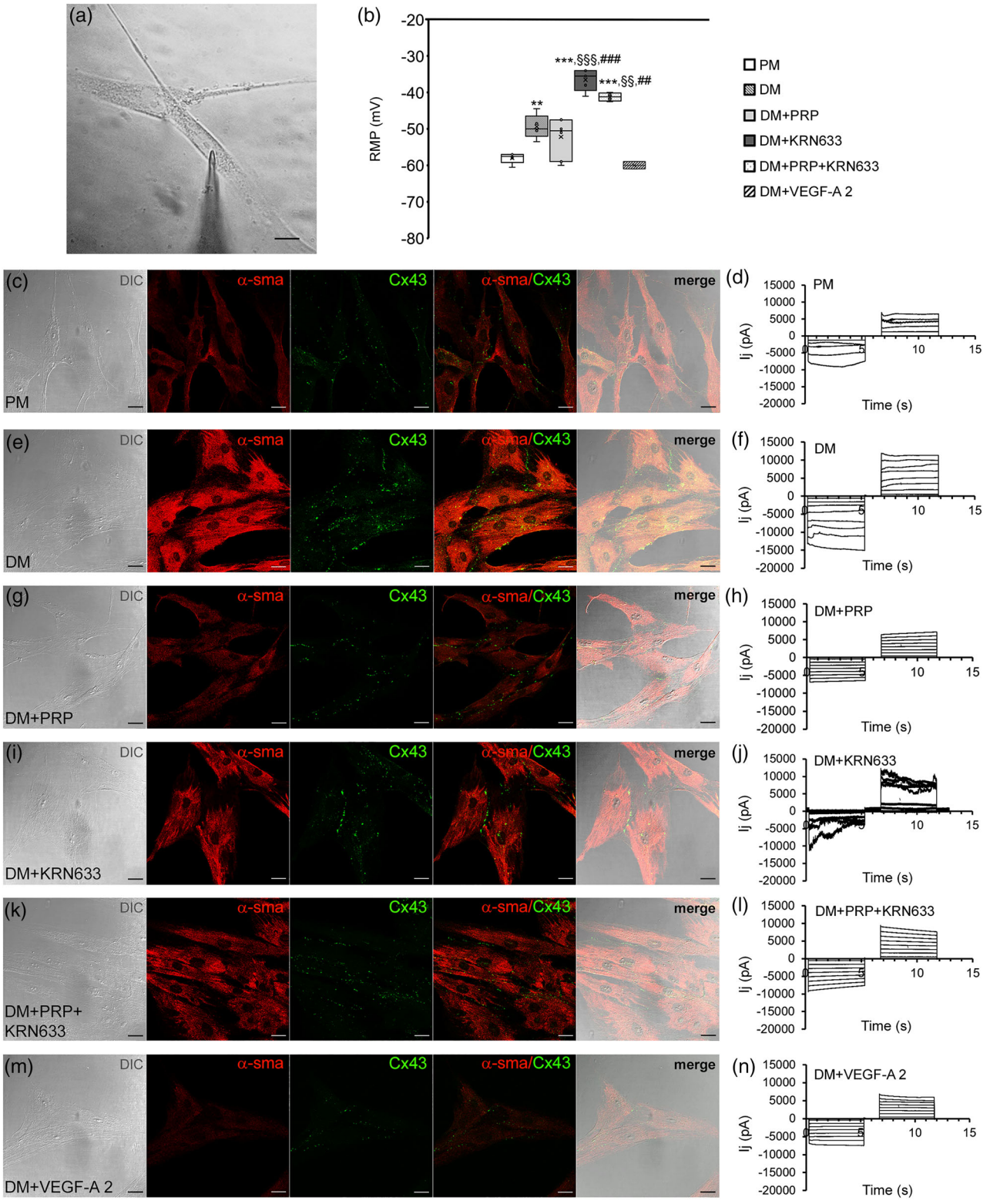

FIGURE 2 Morphofunctional evaluation of human skin primary fibroblasts. (a) Typical human primary skin fibroblasts (in PM) impaled by a patch electrode (scale bar represents 10 μm). (b) Resting membrane potential (RMP, in millivolts; $n = 4$–7 cells; one-way ANOVA with Bonferroni's correction, $P = 0.007$, d.f. = 29; $^{**}P < 0.01$ and $^{***}P < 0.001$ vs. PM; $^{§§}P < 0.01$ and $^{§§§}P < 0.001$ vs. DM; $^{\#\#}P < 0.01$ and $^{\#\#\#}P < 0.001$ vs. DM+PRP) in the indicated experimental conditions. Exact *P*-values of any comparison are reported in Table A6 for clarity. (c,e,g,i,k,m) Representative immunofluorescence analysis of α-sma and Cx43 expression in human cells cultured as specified in Figure 1. Merge: superimposed DIC and fluorescence images (scale bar represents 25 μm). (d,f,h,j,l,n) Representative time course of I_j (in picoamperes) from cell pairs in the indicated experimental conditions. Abbreviations: α-sma, α-smooth muscle actin; Cx43, connexin 43; DIC, differential interference contrast; DM, differentiation medium; I_j, transjunctional current; KRN633, selective pharmacological VEGFR inhibitor; PM, proliferation medium; PRP, platelet-rich plasma; VEGF, vascular endothelial growth factor-A 2 ng/ml

1469445x, 2022, 2, Downloaded from https://physoc.onlinelibrary.wiley.com/doi/10.1113/EP090052 by Universita Di Firenze Sistema, Wiley Online Library on [06/08/2024]. See the Terms and Conditions (https://onlinelibrary.wiley.com/terms-and-conditions) on Wiley Online Library for rules of use; OA articles are governed by the applicable Creative Commons License

cells cultured in DM+VEGF-A 2 showed an increased α-sma expression compared with PM (Figure 1c,l; $n = 60$ ROI, $P = 0.05$).

Morphological and electrophysiological analyses of human fibroblasts cultured in DM+KRN633, DM+PRP+KRN633 or DM+VEGF-A behaved in a similar way to NIH/3T3 fibroblasts, supporting the validity of the NIH/3T3 model and strengthening the above results (Figure 2b,i,k,m). Notably, the RMP values (Figure 2b) estimated from human fibroblasts in DM+KRN633 (−36.5 ± 3.0 mV; $n = 3$) were significantly more positive than those measured in DM (−49.4 ± 3.2 mV; $n = 5$, $P = 0.0001$), suggesting an increased excitability of the cell phenotype under this treatment.

The analysis of I_j evoked by the pulse protocol in Figure 3a applied to NIH/3T3 myofibroblast pairs in DM showed a non-linear time course for negative and positive V_j (Figure 3b), indicating the prevalence of voltage-dependent connexons. Accordingly, myofibroblasts in DM showed higher levels of Cx43 expression compared with undifferentiated cells (Figure 3h,i,s; $n = 60$ ROI, $P < 0.0001$; Table A6), localized in both the cytoplasm and the cell membrane of adjacent cells. In contrast, cell pairs in DM+PRP showed the onset of scarcely voltage-dependent or non-voltage-dependent I_j (Figure 3c), at least at one voltage polarity. This led us to suggest that PRP treatment induced a decrease of voltage-dependent GJs, probably favouring the occurrence of voltage-independent connexons between cell pairs. Consistently, these NIH/3T3 cells in DM+PRP showed a reduced Cx43 expression compared with DM (Figure 3j,s; $n = 60$ ROI, $P < 0.0001$).

The I_j recorded from NIH/3T3 cells in DM+PRP+KRN633 and DM+PRP+AntiVEGF-A Ab (Figure 3e,f) showed a time course different to that observed in DM+PRP and similar to that observed in DM, still suggesting the involvement of voltage-dependent GJs and VEGF-A/VEGFR signalling in the action of PRP on GJ features. Current records from cells in DM+PRP+DMSO or DM+PRP+IgG never gave results different to DM+PRP (data not shown). Accordingly, the increase in Cx43 expression was observed in cells in DM+PRP+KRN633 compared with DM+PRP+DMSO ($n = 60$ ROI, $P < 0.0001$; DM+PRP+DMSO vs. DM+PRP, $P = 1$; DM+PRP+KRN633 vs. DM+PRP, $P < 0.0001$), reaching levels similar to those observed in DM ($n = 60$ ROI, $P = 0.208$) (Figure 3l,n,s). Cells in DM+PRP+AntiVEGF-A Ab showed an increased Cx43 expression compared with cells in DM+PRP+IgG ($n = 60$ ROI, $P < 0.0001$; DM+PRP+IgG vs. DM+PRP $P = 1$; DM+PRP+AntiVEGF-A vs. DM+PRP, $P < 0.0001$); however, this increase was lower than that observed in cells in DM+PRP+KRN633 ($n = 60$ ROI, $P = 0.025$) or DM ($n = 60$ ROI, $P < 0.0001$) (Figure 3o,p,s).

The I_j recorded from NIH/3T3 cells cultured in DM+KRN633 (Figure 3d) was similar to that recorded in DM. Current records from cells in DM+DMSO were similar to those obtained in DM (data not shown). Accordingly, Cx43 expression in these cells was similar to that of cells in DM+DMSO (Figure 3k,m; $n = 60$ ROI, $P = 1$; DM+DMSO vs. DM and DM+KRN633 vs. DM, $P = 1$).

The time course of I_j recorded from fibroblast pairs in DM+VEGF-A 2 or DM+VEGF-A 20 was comparable and, similar to DM+PRP, mostly voltage independent (Figure 3g). Consistent with these electrophysiological findings, NIH/3T3 cells in DM+VEGF-A 2 or 20 showed lower Cx43 expression than those in DM ($n = 60$ ROI, $P < 0.0001$) or DM+PRP ($n = 60$ ROI; DM+VEGF-A 2 $P = 0.0003$, DM+VEGF-A 20 $P = 0.0004$) (Figure 3q,r,s).

To assess the voltage dependence of the overall I_j from NIH/3T3 cells properly, normalized mean values of $I_{j,inst}$ (Figure 4, left-hand panels) and $I_{j,ss}$ (Figure 4, middle panels) were plotted as a function of V_j. The resulting I–V plots clearly showed a different shape compared with those obtained from cells in DM+PRP ($n = 5$) that were linear for both $I_{j,inst}$ (Figure 4a,g,j) and $I_{j,ss}$ (Figure 4b,h,k). Notably, the plot related to DM+PRP+KRN633 ($n = 6$) was steeper than that obtained in DM+PRP alone and showed a sort of shoulder for both negative and positive V_j (Figure 4a,b). Differences between mean current values evoked at any given transjunctional voltage were statistically significant for all the values of V_j except for extreme negative and positive values. For clarity, the exact P-values resulting from the comparisons of each treatment versus DM+PRP are listed in Table A7 for $I_{j,inst}$ and Table A8 for $I_{j,ss}$. This type of behaviour confirmed the prevalence of voltage-dependent connexons in cells cultured in DM+PRP+KRN633. Notably, cells cultured in DM+KRN633 ($n = 11$; Figure 4d,e) demonstrated a voltage dependence of I_j resembling that observed in DM ($n = 7$), which was especially striking for $I_{j,ss}$ (Figure 4e), suggesting a prodifferentiating ability of this milieu. Again, the exact P-values resulting from this comparison are listed in Tables A7 and A8 for $I_{j,inst}$ and $I_{j,ss}$, respectively.

As observed in cells cultured in DM+PRP+KRN633, I_j recorded from fibroblasts in DM+PRP+AntiVEGF-A Ab ($n = 5$) showed a similar behaviour from a qualitative point of view (Figure 4g,h), but had a lower mean amplitude. However, in this condition, statistically significant differences were observed only for $I_{j,ss}$ evoked at −10 and +10 mV (Figure 4h; Tables A7 and A8).

Finally, data related to the $I_{j,inst}$ recorded from cells in DM+VEGF-A 2 showed an almost linear distribution with V_j and overlapped those obtained in DM+PRP (Figure 4j). Data related to $I_{j,ss}$, again, were almost coincident with those obtained in DM+PRP, at least up to +110 mV (Figure 4k), strongly indicating the presence of non-/scarcely voltage-dependent GJ channels.

Conductive properties of the GJs were analysed by the procedure described by Squecco et al. (2020). We calculated instantaneous ($G_{j,inst}$) and steady-state ($G_{j,ss}$) conductances, and $G_{j,ss}/G_{j,inst}$ was plotted as a function of V_j (Figure 4c,f,i,l). Myofibroblasts in DM exhibited an asymmetrical relationship between G_j and V_j ($n = 7$; Figure 4f), which was slightly linear for negative V_j and more bell shaped for positive V_j (see also Squecco et al., 2020). In contrast, G–V plots related to cells in DM+PRP were almost symmetrical and voltage independent in any case, confirming the scarcely voltage-dependent GJs ($n = 5$; Figure 4c,i,l). However, in DM+PRP+KRN633 ($n = 4$; Figure 4c) or DM+PRP+AntiVEGF-A Ab ($n = 5$; Figure 4i), the G–V plot did not show clear linearity, for either negative or positive V_j, suggesting that hindering VEGF-A activity or its receptor functionality prevented the efficacy of PRP in altering the Cx expression and their docking into scarcely voltage-dependent GJs. Lastly, the G–V plot analysis also indicated a similar behaviour for cell pairs in DM+VEGF-A 2 and DM+PRP (Figure 4l). Similar results were obtained in DM+VEGF-A

1469445x, 2022, 2, Downloaded from https://physoc.onlinelibrary.wiley.com/doi/10.1113/EP090052 by Universita Di Firenze Sistema, Wiley Online Library on [06/08/2024]. See the Terms and Conditions (https://onlinelibrary.wiley.com/terms-and-conditions) on Wiley Online Library for rules of use; OA articles are governed by the applicable Creative Commons License

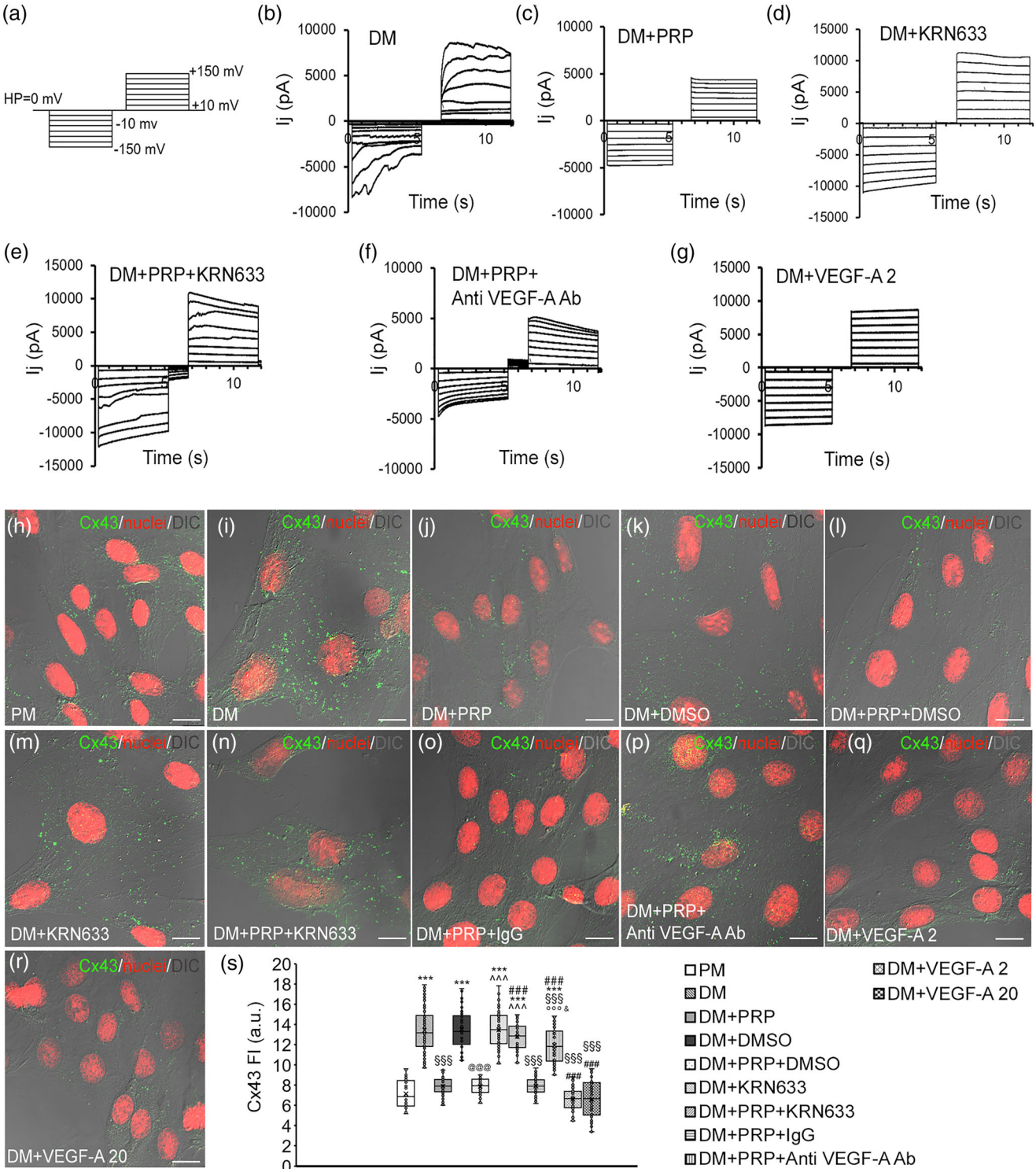

FIGURE 3 Time course of transjunctional currents (I_j) and confocal immunofluorescence analysis of connexin 43 (Cx43) expression in NIH/3T3 fibroblasts. (a) Bipolar voltage pulse protocol applied to NIH/3T3 cell pairs. (b–g) Typical time course of I_j (in picoamperes) from cell pairs in the indicated experimental conditions as specified in Figure 1. (h–r) Representative superimposed differential interference contrast (DIC) and confocal fluorescence images acquired simultaneously of the NIH/3T3 cells cultured as in Figure 1, immunostained for Cx43 and counterstained with propidium iodide to label nuclei. Scale bar represents 10 μm. (s) Densitometric analysis of the fluorescence intensity (FI, in arbitrary units) of Cx43. Values represent the mean ± SD. Significance of difference ($n = 60$ regions of interest; one-way ANOVA with Tukey's post hoc test): *** versus PM ($P < 0.0001$); §§§ versus DM ($P < 0.0001$); $^{###}$ versus DM+PRP ($P < 0.0001$; VEGF-A 2, $P = 0.0003$; VEGF-A 20, $P = 0.0004$); $^{@@@}$ versus DM+DMSO; $^{\wedge\wedge\wedge}$ versus DM+PRP+DMSO ($P < 0.0001$); $^{\&}$ versus DM+PRP+KRN ($P = 0.025$); $^{\circ\circ\circ}$ versus DM+PRP+IgG ($P < 0.0001$). Abbreviations as in the Figure 1

1469445x, 2022, 2, Downloaded from https://physoc.onlinelibrary.wiley.com/doi/10.1113/EP090052 by Universita Di Firenze Sistema, Wiley Online Library on [06/08/2024]. See the Terms and Conditions (https://onlinelibrary.wiley.com/terms-and-conditions) on Wiley Online Library for rules of use; OA articles are governed by the applicable Creative Commons License

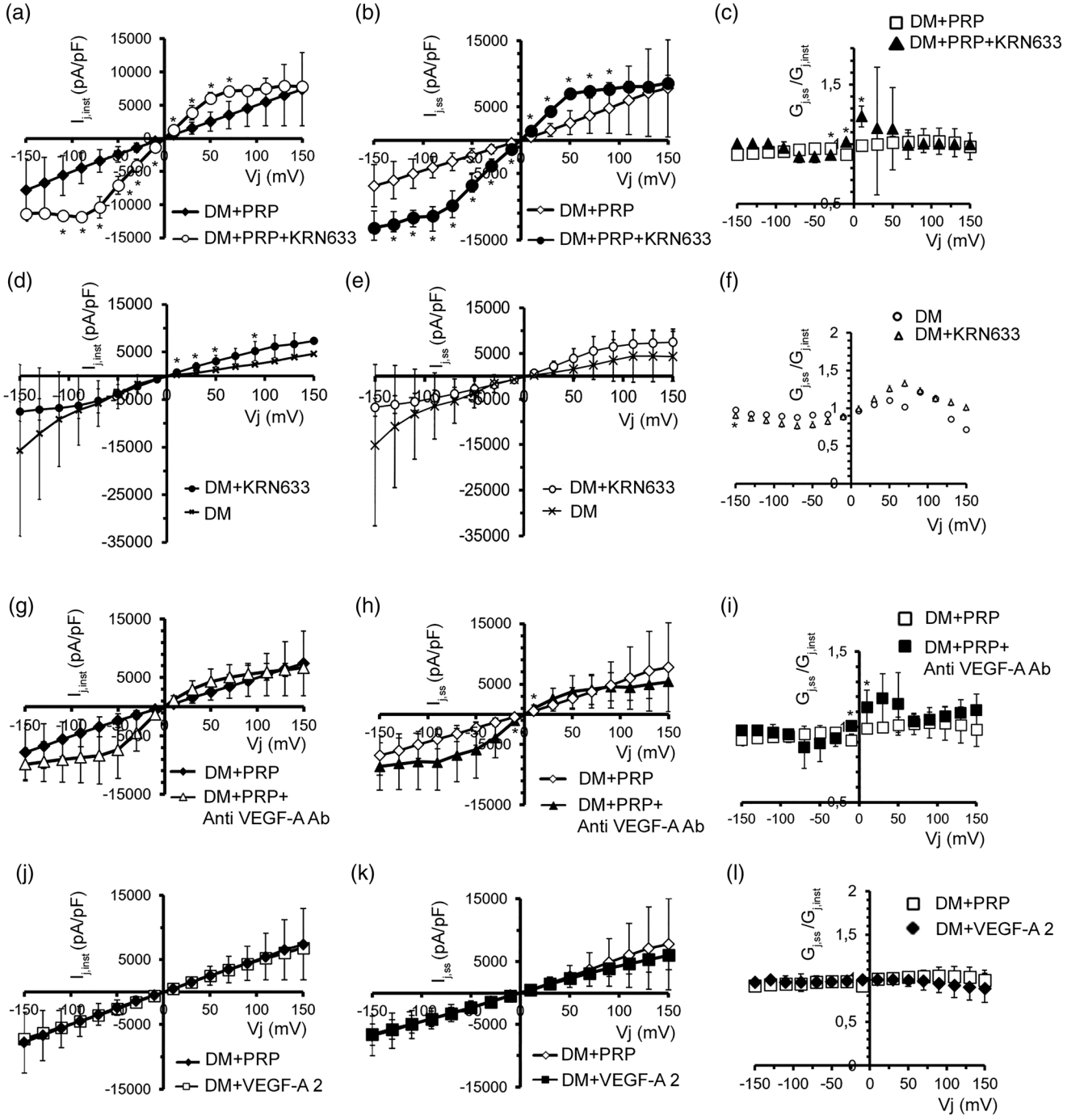

FIGURE 4 Voltage dependence of transjunctional currents (I_j) and conductance (G_j) from NIH/3T3 cell pairs. Normalized $I_{j,inst}$ values (a,d,g,j) and $I_{j,ss}$ values (b,e,h,k). The I_j values (in picoamperes per picofarad) are plotted versus V_j (in millivolts), recorded from NIH/3T3 cell pairs cultured as specified in Figure 1 in DM+PRP (a,b,g,h,j,k, $n = 14$), DM+PRP+KRN633 (a,b, $n = 6$), DM+KRN633 (d,e, $n = 11$), DM+PRP+AntiVEGF-A Ab (g,h, $n = 5$) and DM+VEGF-A 2 (j,k, $n = 6$). Note the almost linear voltage dependence of I_j in DM+PRP for both $I_{j,inst}$ and $I_{j,ss}$. (c,f,i,l) Voltage dependence of G_j estimated by plotting $G_{j,ss}/G_{j,inst}$ versus V_j (in millivolts), related to DM+PRP (c,i,l, $n = 14$), DM (f, $n = 7$), DM+KRN633 (f, $n = 11$), DM+PRP+KRN633 (c, $n = 4$), DM+PRP+AntiVEGF-A Ab (i, $n = 5$) and DM+VEGF-A 2 (l, $n = 6$). Values represent the mean ± SD. Error bars are visible if they exceed the symbol size. $^*P < 0.05$ (Student's unpaired t-test). Abbreviations as in the Figure 1

1469445x, 2022, 2, Downloaded from https://physoc.onlinelibrary.wiley.com/doi/10.1113/EP090052 by Universita Di Firenze Sistema, Wiley Online Library on [06/08/2024]. See the Terms and Conditions (https://onlinelibrary.wiley.com/terms-and-conditions) on Wiley Online Library for rules of use; OA articles are governed by the applicable Creative Commons License

20 (not shown). The exact *P*-values resulting from all the comparisons depicted in Figure 4c,f,i,l at any given V_j are listed in Table A9 for clarity.

Remarkably, the recordings of the time course of I_j and the analysis of Cx43 expression performed in human fibroblasts cultured in various experimental conditions revealed responses comparable to those elicited in NIH/3T3 fibroblasts, corroborating the above results and conclusions (Figure 2c–n).

4 | DISCUSSION

The current antifibrotic therapeutic options have limited efficacy; hence, there is an urgent need to identify effective treatments. Supporting the antifibrotic potential of PRP, this study has a potential clinical interest; it gives new insight into the mechanisms of action of PRP and contributes to identifying possible smart therapeutic targets represented by the GJ and Cx43.

We corroborate the ability of PRP to hinder TGF-β1-induced morphofunctional differentiation of fibroblasts (either the murine NIH/3T3 cell line or primary human adult skin fibroblasts) towards myofibroblasts via VEGF-A/VEGFR signalling, extending our previous observations (Chellini et al., 2018; Squecco et al., 2020). The ability of primary adult human skin fibroblasts to show morphofunctional responses to different treatments similar to those of the murine cell line strengthens the findings of this research and enhances their clinical relevance.

Based on published results showing that NIH/3T3 cells, in our experimental model, expressed only VEGFR-1, and not VEGFR-2 or VEGFR-3 (Chellini et al., 2018), we can be confident of the involvement of VEGFR-1 in the cell responses observed in the present study. Concerning RMP, a parameter useful as an index of differentiation that is strictly related to cell excitability and contractility, the effect of PRP and of the other treatments tested here is not clear cut.

As expected, myofibroblasts showed a more depolarized RMP compared with fibroblasts (Squecco et al., 2015) and although PRP treatment showed a tendency to repolarize its value, the effect was not striking. Moreover, the trend to membrane repolarization also observed in the presence of PRP and blocking VEGF-A/VEGFR agents suggests that the alterations in RMP owing to PRP do not strictly involve VEGF-A and its receptor. This led us to hypothesize that other bioactive molecules in PRP might determine either synergistic or antagonistic effects, with the engagement of different effector/receptor systems in determining the outcome on RMP, probably involving a long-term modulation of membrane ion channels and/or pumps. In this regard, preliminary experiments in our laboratory showed that sphingosine 1-phosphate, a bioactive lipid supposed to be released by activated PRP (Hoeferlin et al., 2015) and recognized as a profibrotic agent (Donati et al., 2021), is able to depolarize RMP, possibly antagonizing the effects of VEGF-A. This is another aspect that certainly deserves further investigation. In contrast, for all the analysed morphological features indicative of a myofibroblastic phenotype, PRP appears effective in hampering them, and VEGF-A or VEGFR inhibition prevents PRP-promoted antifibrotic effects. Notably, VEGFR inhibition seems to elicit more marked effects than VEGF-A neutralization, suggesting a potential role of other VEGFR-1 ligands, such as VEGF-B or placental growth factor, in mediating the cell response to PRP. Further experiments are ongoing in our laboratory to assess the presence of such ligands in PRP samples and, in case, their possible effects on fibroblast response.

As far as data related to the treatment of differentiating human cells with KRN633 are concerned, they show the acquisition of a typical myofibroblastic phenotype by the cells, with an even more depolarized RMP compared with that of myofibroblasts cultured in DM alone, which could lead to an increased excitability of these cells and a more functional phenotype. This is not surprising, because the differentiated status can be associated with the neo-expression of membrane proteins and ion channels, as stated by Chatelier et al. (2012), who found a fourfold increase in the expression of $Na_v1.5$ α-subunit transcripts in human atrial myofibroblasts associated with fast inward voltage-gated sodium currents when compared with fibroblasts. We can speculate that when VEGFR is inhibited, profibrotic pathways might be enhanced, and we hypothesize the existence of a potential antagonistic cross-talk between TGF-β1- and VEGFR-mediated signalling. In other words, VEGFR might interfere negatively with the TGF-β1 pathway or also with the action of other non-canonical profibrotic factors. These observations might contribute to support the antifibrotic role of the VEGFR pathway. However, the clear-cut role of VEGF-A signalling has been confirmed here by treatment of cells with soluble VEGF-A.

Furthermore, we show here that PRP prevents the onset of TGF-β1-driven voltage-dependent GJ currents and the increase of Cx43 expression during fibroblast myo-differentiation, hampering the direct transmission of electrical and metabolic signals. These data, in addition to corroborating our previous observations (Squecco et al., 2020), highlight, for the first time, that these effects on the gap junctions are mediated by VEGF-A/VEGFR.

Transforming growth factor-β1 has recognized pleiotropic effects on the electrical myofibroblast phenotype, altering several ion channels, pumps and Cx transcripts (Salvarani et al., 2017). Notably, TGF-β1 induces an increase of Cx43 that allows the myofibroblasts to couple electrically with the functional tissue-specific cell type; nonetheless, it might have undesirable consequences. In the cardiac tissue, for instance, where Cx43 is the most abundant isoform of GJs (Zhang et al., 2020), myofibroblasts can cause a substantial TGF-β1-dependent depolarization of the cardiomyocytes, as a result of electrotonic cross-talk that results in a detrimental arrhythmogenic condition (Nagaraju et al., 2019).

It is worth noting that Cx expression and modulation of activity are always crucial to cellular function, and many diseases are ascribed to changes in the synthesis and/or function of these fundamental proteins. Given that Cx43 is almost ubiquitous and can undoubtedly be considered a target of interest for controlling the fibrotic response, any intervention aimed to decrease Cx43 expression and GJ functionality might be beneficial in counteracting harmful effects of fibrosis.

In this regard, our findings allow us to assert that PRP might offer a promising therapeutic option. To our knowledge, this is the first

1469445x, 2022, 2, Downloaded from https://physoc.onlinelibrary.wiley.com/doi/10.1113/EP090052 by Universita Di Firenze Sistema, Wiley Online Library on [06/08/2024]. See the Terms and Conditions (https://onlinelibrary.wiley.com/terms-and-conditions) on Wiley Online Library for rules of use; OA articles are governed by the applicable Creative Commons License

study to assess the involvement of VEGF-A/VEGFR signalling in the GJ communication to counteract fibroblast-to-myofibroblast transition.

Collectively, our results recognize GJs and Cx43 as crucial targets of the VEGF-A/VEGFR antifibrotic pathway, thereby providing cues for the development of new therapies. Remarkably, although the use of PRP is promising, it remains debated. This is mainly attributable to scarce clarification of the cellular and molecular mechanisms underpinning its action, to the lack of definitive guidelines for PRP preparation and a thorough characterization of its composition (Collins et al., 2021).

We are aware of the limitations of our study essentially linked to the in vitro experimentation, including the use of standard plastic culture plates, which do not allow us to accomplish the control for biomechanical activation of fibroblasts that is an additional key stimulus for fibroblast-to-myofibroblast transition (Pakshir et al., 2020). Accordingly, we are planning experiments to culture the cells on 'tissue-soft' plates (Young's modulus of 5–10 kPa, as opposed to plastic plates, which are orders of magnitude more stiff).

To conclude, despite all these considerations, this study provides the essential groundwork for further investigation on the morphofunctional characterization of myofibroblasts and the effects of PRP in the setting of fibrosis. In this regard, in addition to electrical coupling between paired (myo)fibroblasts, future studies will be planned to go beyond and address the role of PRP in Cx43-mediated coupling between (myo)fibroblasts and cardiomyocytes.

ACKNOWLEDGEMENTS

We wish to thank Professor M. Manetti for kindly providing human primary skin fibroblasts, Dr E. Idrizaj for assistance with electrophysiological experiments, F. Palmieri for additional data analysis and Dr I. P. Lamminpaa for grammatical revisions. This research was supported by the annual financing fund by MIUR (Ministry of Education, University and Research, Italy), University of Florence to C.S., F.C., S.Z.-O. and R.S. and by FFABR-MIUR 2017 (Financing Fund for Basic Research Activities) granted to C.S. and R.S.

COMPETING INTERESTS

None declared.

AUTHOR CONTRIBUTIONS

The experiments were performed in the laboratories of the sections of Physiological Sciences and Anatomy of the Department of Experimental and Clinical Medicine, University of Florence, Italy and in the laboratory of the Transfusion Medicine and Cell Therapy Unit at 'A. Meyer' University Children's Hospital, Florence, Italy. Conceptualization, C.S. and R.S.; data curation, C.S., R.G., F.C., A.T. and R.S.; formal analysis, C.S., F.C. and R.S.; funding acquisition, C.S., F.C., S.Z.-O. and R.S.; investigation, C.S., R.G., F.C., A.T. and R.S.; resources, C.S., F.C., P.P., F.B., S.Z.-O. and R.S.; visualization, C.S., R.G., F.C., A.T. and R.S.; writing, original draft preparation, C.S. and R.S.; writing, review and editing, C.S., R.G., F.C., A.T., S.Z.-O. and R.S. All authors approved the final version of the manuscript and agree to be accountable for all aspects of the work in ensuring that questions related to the accuracy or integrity of any part of the work are appropriately investigated and resolved. All persons designated as authors qualify for authorship, and all those who qualify for authorship are listed.

DATA AVAILABILITY STATEMENT

The data that support the findings of this study are available on request from the corresponding author.

ORCID

Roberta Squecco https://orcid.org/0000-0002-6534-3675

REFERENCES

Chatelier, A., Mercier, A., Tremblier, B., Thériault, O., Moubarak, M., Benamer, N., Corbi, P., Bois, P., Chahine, M., & Faivre, J. F. (2012). A distinct *de novo* expression of $Na_v1.5$ sodium channels in human atrial fibroblasts differentiated into myofibroblasts. *The Journal of Physiology*, *590*(17), 4307–4319. https://doi.org/10.1113/jphysiol.2012.233593

Chellini, F., Tani, A., Vallone, L., Nosi, D., Pavan, P., Bambi, F., & Sassoli, C. (2018). Platelet-rich plasma prevents in vitro transforming growth factor-β1-induced fibroblast to myofibroblast transition: Involvement of vascular endothelial growth factor (VEGF)-A/VEGF receptor-1-mediated signaling. *Cells*, *7*(9), 142. https://doi.org/10.3390/cells7090142

Chellini, F., Tani, A., Zecchi-Orlandini, S., Giannelli, M., & Sassoli, C. (2020). In vitro evidences of different fibroblast morpho-functional responses to red, near-infrared and violet-blue photobiomodulation: Clues for addressing wound healing. *Applied Science*, *10*, 7878. https://doi.org/10.3390/app10217878

Chellini, F., Tani, A., Zecchi-Orlandini, S., & Sassoli, C. (2019). Influence of platelet-rich and platelet-poor plasma on endogenous mechanisms of skeletal muscle repair/regeneration. *International Journal of Molecular Sciences*, *20*(3), 683. https://doi.org/10.3390/ijms20030683

Collins, T., Alexander, D., & Barkatali, B. (2021). Platelet-rich plasma: A narrative review. *EFORT Open Reviews*, *6*(4), 225–235. https://doi.org/10.1302/2058-5241.6.200017

Donati, C., Cencetti, F., Bernacchioni, C., Vannuzzi, V., & Bruni, P. (2021). Role of sphingosine 1-phosphate signalling in tissue fibrosis. *Cellular Signalling*, *78*, 109861. https://doi.org/10.1016/j.cellsig.2020.109861

Guillodo, Y., Madouas, G., Simon, T., Le Dauphin, H., & Saraux, A. (2016). Platelet-rich plasma (PRP) treatment of sports-related severe acute hamstring injuries. *Muscles, Ligaments and Tendons Journal*, *05*, 284–288. https://doi.org/10.11138/mltj/2015.5.4.284. https://doi.org/10.32098/mltj.04.2015.06

Hoeferlin, L. A., Huynh, Q. K., Mietla, J. A., Sell, S. A., Tucker, J., Chalfant, C. E., & Wijesinghe, D. S. (2015). The lipid portion of activated platelet-rich plasma significantly contributes to its wound healing properties. *Advances in Wound Care*, *4*, 100–109. https://doi.org/10.1089/wound.2014.0589

Lynch, M. D., & Bashir, S. (2016). Applications of platelet-rich plasma in dermatology: A critical appraisal of the literature. *The Journal of Dermatological Treatment*, *27*(3), 285–289. https://doi.org/10.3109/09546634.2015.1094178

Miao, H., Wu, X.-Q., Zhang, D.-D., Wang, Y.-N., Guo, Y., Li, P., & Zhao, Y.-Y. (2021). Deciphering the cellular mechanisms underlying fibrosis-associated diseases and therapeutic avenues. *Pharmacological Research*, *163*, 105316. https://doi.org/10.1016/j.phrs.2020.105316

Moghadam, A., Khozani, T. T., Mafi, A., Namavar, M. R., & Dehghani, F. (2017). Effects of platelet-rich plasma on kidney regeneration in gentamicin-induced nephrotoxicity. *Journal of Korean Medical Science*, *32*(1), 13–21. https://doi.org/10.3346/jkms.2017.32.1.13

Nagaraju, C. K., Dries, E., Gilbert, G., Abdesselem, M., Wang, N., Amoni, M., & Sipido, K. R. (2019). Myofibroblast modulation of cardiac myocyte

1469445x, 2022, 2, Downloaded from https://physoc.onlinelibrary.wiley.com/doi/10.1113/EP090052 by Universita Di Firenze Sistema, Wiley Online Library on [06/08/2024]. See the Terms and Conditions (https://onlinelibrary.wiley.com/terms-and-conditions) on Wiley Online Library for rules of use; OA articles are governed by the applicable Creative Commons License

structure and function. *Scientific Reports*, *9*(1), 8879. https://doi.org/10.1038/s41598-019-45078-2

Pakshir, P., Noskovicova, N., Lodyga, M., Son, D. O., Schuster, R., Goodwin, A., & Hinz, B. (2020). The myofibroblast at a glance. *Journal of Cell Science*, *133*(13), jcs227900. https://doi.org/10.1242/jcs.227900

Romano, E., Rosa, I., Fioretto, B. S., Lucattelli, E., Innocenti, M., Ibba-Manneschi, L., Matucci-Cerinic, M., & Manetti, M. (2020). A two-step immunomagnetic microbead-based method for the isolation of human primary skin telocytes/CD34+ stromal cells. *International Journal of Molecular Sciences*, *21*(16), 5877. https://doi.org/10.3390/ijms21165877

Salvarani, N., Maguy, A., De Simone, S. A., Miragoli, M., Jousset, F., & Rohr, S. (2017). TGF-β_1 (transforming growth factor-β_1) plays a pivotal role in cardiac myofibroblast arrhythmogenicity. *Circulation. Arrhythmia and Electrophysiology*, *10*(5), e004567. https://doi.org/10.1161/CIRCEP.116.004567

Sassoli, C., Nistri, S., Chellini, F., & Bani, D. (2021). Human recombinant relaxin (serelaxin) as anti-fibrotic agent: Pharmacology, limitations and actual perspectives. *Current Molecular Medicine*, Advance online publication. https://doi.org/10.2174/1566524021666210309113650

Sassoli, C., Pini, A., Chellini, F., Mazzanti, B., Nistri, S., Nosi, D., Saccardi, R., Quercioli, F., Zecchi-Orlandini, S., & Formigli, L. (2012). Bone marrow mesenchymal stromal cells stimulate skeletal myoblast proliferation through the paracrine release of VEGF. *PLoS One*, *7*(7), e37512. https://doi.org/10.1371/journal.pone.0037512

Schroeder, C. C., Scariot, J. S., Ribeiro, J. C., Deliberador, T. M., & Giovanini, A. M. (2016). Platelet rich plasma (PRP) produces an atherofibrotic histophenotype during craniofacial bone repair due to changes of immunohistochemical expression of Erk1/2, p38α/β, adiponectin and elevated presence of cells exhibiting B-scavenger receptor (CD36+). *Brazilian Dental Journal*, *27*, 243–254. https://doi.org/10.1590/0103-6440201602450

Shoeib, H. M., Keshk, W. A., Foda, A. M., & Abo El Noeman, S. E. (2018). A study on the regenerative effect of platelet-rich plasma on experimentally induced hepatic damage in albino rats. *Canadian Journal of Physiology and Pharmacology*, *96*(6), 630–636. https://doi.org/10.1139/cjpp-2017-0738

Squecco, R., Chellini, F., Idrizaj, E., Tani, A., Garella, R., Pancani, S., & Sassoli, C. (2020). Platelet-rich plasma modulates gap junction functionality and connexin 43 and 26 expression during TGF-β1-induced fibroblast to myofibroblast transition: Clues for counteracting fibrosis. *Cells*, *9*(5), 1199. https://doi.org/10.3390/cells9051199

Squecco, R., Sassoli, C., Garella, R., Chellini, F., Idrizaj, E., Nistri, S., & Francini, F. (2015). Inhibitory effects of relaxin on cardiac fibroblast-to-myofibroblast transition: An electrophysiological study. *Experimental Physiology*, *100*(6), 652–666. https://doi.org/10.1113/EP085178

Vu, T. D., Pal, S. N., Ti, L. K., Martinez, E. C., Rufaihah, A. J., Ling, L. H., & Kofidis, T. (2015). An autologous platelet-rich plasma hydrogel compound restores left ventricular structure, function and ameliorates adverse remodeling in a minimally invasive large animal myocardial restoration model: A translational approach: Vu and Pal "Myocardial Repair: PRP, Hydrogel and Supplements". *Biomaterials*, *45*, 27–35. https://doi.org/10.1016/j.biomaterials.2014.12.013

Xu, Y., Hu, J., Yilmaz, D. E., & Bachman, S. (2021). Connexin43 is differentially distributed within renal vasculature and mediates profibrotic differentiation in medullary fibroblasts. *American Journal of Physiology. Renal Physiology*, *320*(1), F17–F30. https://doi.org/10.1152/ajprenal.00453.2020

Zhang, Y., Hou, M.-C., Li, J.-J., Qi, Y., Zhang, Y., She, G., Ren, Y.-J., Wu, W., Pang, Z.-D., Xie, W., Deng, X.-L., & Du, X.-J. (2020). Cardiac β-adrenergic receptor activation mediates distinct and cell type-dependent changes in the expression and distribution of connexin 43. *Journal of Cellular and Molecular Medicine*, *24*(15), 8505–8517. https://doi.org/10.1111/jcmm.15469

SUPPORTING INFORMATION

Additional supporting information may be found in the online version of the article at the publisher's website.

How to cite this article: Sassoli, C., Garella, R., Chellini, F., Tani, A., Pavan, P., Bambi, F., Zecchi-Orlandini, S., & Squecco, R. (2022). Platelet-rich plasma affects gap junctional features in myofibroblasts in vitro via vascular endothelial growth factor (VEGF)-A/VEGF receptor. *Experimental Physiology*, *107*, 106–121. https://doi.org/10.1113/EP090052

1469445x, 2022, 2, Downloaded from https://physoc.onlinelibrary.wiley.com/doi/10.1113/EP090052 by Universita Di Firenze Sistema, Wiley Online Library on [06/08/2024]. See the Terms and Conditions (https://onlinelibrary.wiley.com/terms-and-conditions) on Wiley Online Library for rules of use; OA articles are governed by the applicable Creative Commons License

APPENDIX

TABLE A1 *P*-Values resulting from the comparisons of resting membrane potential values measured from NIH/3T3 murine fibroblasts in the different conditions

	PM	DM	DM+ PRP	DM+ DMSO	DM+ DMSO+ PRP	DM+ KRN633	DM+ PRP+ KRN633	DM+ PRP+ IgG	DM+PRP+ AntiVEGF-A Ab	DM+ VEGF-A 2	DM+ VEGF-A 20
vs. PM	—	0.059	0.396	0.077	0.325	0.069	0.756	0.188	0.562	0.149	0.412
vs. DM		—	0.463	0.655	0.296	0.754	0.013	0.327	0.0104	0.287	0.007
vs. DM+PRP			—	0.556	0.967	0.505	0.472	0.859	0.586	0.802	0.692
vs. DM+DMSO				—	0.388	0.788	0.021	0.466	0.019	0.449	0.015
vs. DM+DMSO+PRP					—	0.333	0.372	0.771	0.497	0.687	0.622
vs. DM+KRN633						—	0.016	0.369	0.010	0.316	**0.0005**
vs. DM+KRN633+PRP							—	0.161	0.697	0.090	0.413
vs. DM+PRP+IgG								—	0.226	0.910	0.291
vs. DM+PRP+AntiVEGF-A Ab									—	0.121	0.638
vs. DM+VEGF-A 2										—	0.145
vs. DM+VEGF-A 20											—

Note. Differences were assessed by one-way ANOVA followed by Bonferroni's post hoc test. Statistical significance is shown in bold.
Abbreviations: PM, proliferation medium; DM, differentiation medium; PRP, platelet-rich plasma; KRN633, selective pharmacological VEGFR inhibitor; IgG, irrelevant isotype-matched IgG; Anti VEGF-A, vascular endothelial growth factor-A; Ab, anti-VEGF-A neutralizing antibodies; VEGF-A 2, 20, soluble VEGF-A 2 or 20 ng/ml.

TABLE A2 *P*-Values resulting from the comparisons of the amount of α-smooth muscle actin fluorescent signal (in arbitrary units) from NIH/3T3 murine fibroblasts in the different conditions

	PM	DM	DM+ PRP	DM+ DMSO	DM+ DMSO+ PRP	DM+ KRN633	DM+ PRP+ KRN633	DM+ PRP+ IgG	DM+PRP+ AntiVEGF-A Ab	DM+ VEGF-A 2	DM+ VEGF-A 20
vs. PM	—	< **0.0001**	0.890	< **0.0001**	0.804	< **0.0001**	< **0.0001**	1	< **0.0001**	**0.05**	1
vs. DM		—	< **0.0001**	1	< **0.0001**	1	1	< **0.0001**	**0.007**	< **0.0001**	< **0.0001**
vs. DM+PRP			—	< **0.0001**	1	< **0.0001**	< **0.0001**	0.983	< **0.0001**	0.627	0.806
vs. DM+DMSO				—	< **0.0001**	1	1	< **0.0001**	**0.004**	< **0.0001**	< **0.0001**
vs. DM+DMSO+ PRP					—	< **0.0001**	< **0.0001**	0.952	< **0.0001**	0.742	0.7
vs. DM+KRN633						—	1	< **0.0001**	**0.006**	< **0.0001**	< **0.0001**
vs. DM+KRN633+ PRP							—	< **0.0001**	**0.019**	< **0.0001**	< **0.0001**
vs. DM+PRP+IgG								—	< **0.0001**	0.111	1
vs. DM+PRP+AntiVEGF-A Ab									—	< **0.0001**	< **0.0001**
vs. DM+VEGF-A 2										—	**0.033**
vs. DM+VEGF-A 20											—

Note. Differences were assessed by one-way ANOVA followed by Tukey's post hoc test. Statistical significance is shown in bold. All abbreviations are mentioned in the footnote to Table A1.

1469445x, 2022, 2, Downloaded from https://physoc.onlinelibrary.wiley.com/doi/10.1113/EP090052 by Universita Di Firenze Sistema, Wiley Online Library on [06/08/2024]. See the Terms and Conditions (https://onlinelibrary.wiley.com/terms-and-conditions) on Wiley Online Library for rules of use; OA articles are governed by the applicable Creative Commons License

TABLE A3 *p*-Values resulting from the comparisons of the amount of vinculin fluorescent signal (in arbitrary units) from NIH/3T3 murine fibroblasts in the different conditions

	PM	DM	DM+ PRP	DM+ DMSO	DM+ DMSO+ PRP	DM+ KRN633	DM+ PRP+ KRN633	DM+ PRP+ IgG	DM+PRP+ AntiVEGF-A Ab	DM+ VEGF-A 2	DM+ VEGF-A 20
vs. PM	—	< **0.0001**	1	< **0.0001**	1	< **0.0001**	< **0.0001**	0.703	< **0.0001**	0.585	0.688
vs. DM		—	< **0.0001**	1	< **0.0001**	1	0.701	< **0.0001**	**0.049**	< **0.0001**	< **0.0001**
vs. DM+PRP			—	< **0.0001**	1	< **0.0001**	< **0.0001**	0.789	< **0.0001**	0.679	0.776
vs. DM+DMSO				—	< **0.0001**	1	0.627	< **0.0001**	**0.038**	< **0.0001**	< **0.0001**
vs. DM+DMSO+PRP					—	< **0.0001**	< **0.0001**	0.697	< **0.0001**	0.579	0.682
vs. DM+KRN633						—	0.663	< **0.0001**	**0.043**	< **0.0001**	< **0.0001**
vs. DM+KRN633+ PRP							—	< **0.0001**	0.836	< **0.0001**	< **0.0001**
vs. DM+PRP+IgG								—	< **0.0001**	1	1
vs. DM+PRP+AntiVEGF-A Ab									—	< **0.0001**	< **0.0001**
vs. DM+VEGF-A 2										—	1
vs. DM+VEGF-A 20											—

Note. Differences were assessed by one-way ANOVA followed by Tukey's post hoc test. Statistical significance is shown in bold. All abbreviations are mentioned in the footnote to Table A1.

TABLE A4 *P*-Values resulting from the comparisons of the cell surface area (in arbitrary units) from NIH/3T3 murine fibroblasts in the different conditions

	PM	DM	DM+ PRP	DM+ DMSO	DM+ DMSO+ PRP	DM+ KRN633	DM+ PRP+ KRN633	DM+ PRP+ IgG	DM+PRP+ AntiVEGF-A Ab	DM+ VEGF-A 2	DM+ VEGF-A 20
vs. PM	—	< **0.0001**	1	< **0.0001**	1	< **0.0001**	< **0.0001**	**0.026**	< **0.0001**	0.841	0.746
vs. DM		—	< **0.0001**	1	< **0.0001**	1	0.926	< **0.0001**	0.950	< **0.0001**	< **0.0001**
vs. DM+PRP			—	< **0.0001**	1	< **0.0001**	< **0.0001**	0.071	< **0.0001**	0.978	0.944
vs. DM+DMSO				—	< **0.0001**	1	0.639	< **0.0001**	0.692	< **0.0001**	< **0.0001**
vs. DM+DMSO+ PRP					—	< **0.0001**	< **0.0001**	0.099	< **0.0001**	0.992	0.975
vs. DM+KRN633						—	0.737	< **0.0001**	0.785	< **0.0001**	< **0.0001**
vs. DM+KRN633+ PRP							—	< **0.0001**	1	< **0.0001**	< **0.0001**
vs. DM+PRP+IgG								—	< **0.0001**	0.517	0.63
vs. DM+PRP+AntiVEGF-A Ab									—	< **0.0001**	< **0.0001**
vs. DM+VEGF-A 2										—	1
vs. DM+VEGF-A 20											—

Note. Differences were assessed by one-way ANOVA followed by Tukey's post hoc test. Statistical significance is shown in bold. All abbreviations are mentioned in the footnote to Table A1.

TABLE A5 *P*-Values resulting from the comparisons of resting membrane potential values measured from primary human adult skin fibroblasts in the different conditions

	PM	DM	DM+PRP	DM+KRN633	DM+KRN633+PRP	DM+VEGF-A 2
vs. PM	–	**0.002**	0.025	< **0.0001**	< **0.0001**	0.221
vs. DM		–	0.276	**0.0001**	**0.003**	0.471
vs. DM+PRP			–	< **0.0001**	**0.001**	0.369
vs. DM+KRN633				–	0.020	0.819
vs. DM+KRN633+PRP					–	0.893
vs. DM+VEGF-A 2						–

Note. Differences were assessed by one-way ANOVA followed by Bonferroni's post hoc test. Statistical significance is shown in bold. All abbreviations are mentioned in the footnote to Table A1.

1469445x, 2022, 2, Downloaded from https://physoc.onlinelibrary.wiley.com/doi/10.1113/EP090052 by Universita Di Firenze Sistema, Wiley Online Library on [06/08/2024]. See the Terms and Conditions (https://onlinelibrary.wiley.com/terms-and-conditions) on Wiley Online Library for rules of use; OA articles are governed by the applicable Creative Commons License

TABLE A6 *P*-Values resulting from the comparisons of the amount of Cx43 fluorescent signal (in arbitrary units) from NIH/3T3 murine fibroblasts in the different conditions

	PM	DM	DM+ PRP	DM+ DMSO	DM+ DMSO+ PRP	DM+ KRN633	DM+ PRP+ KRN633	DM+ PRP+ IgG	DM+PRP+ AntiVEGF-A Ab	DM+ VEGF-A 2	DM+ VEGF-A 20
vs. PM	—	< **0.0001**	0.075	< **0.0001**	0.088	< **0.0001**	< **0.0001**	0.076	< **0.0001**	0.396	0.425
vs. DM		—	< **0.0001**	1	< **0.0001**	1	0.208	< **0.0001**	< **0.0001**	< **0.0001**	< **0.0001**
vs. DM+PRP			—	< **0.0001**	1	< **0.0001**	< **0.0001**	1	< **0.0001**	**0.0003**	**0.0004**
vs. DM+DMSO				—	< **0.0001**	1	0.106	< **0.0001**	< **0.0001**	< **0.0001**	< **0.0001**
vs. DM+DMSO+ PRP					—	< **0.0001**	< **0.0001**	1	< **0.0001**	**0.0004**	**0.0004**
vs. DM+KRN633						—	0.163	< **0.0001**	< **0.0001**	< **0.0001**	< **0.0001**
vs. DM+KRN633+ PRP							—	< **0.0001**	**0.025**	< **0.0001**	< **0.0001**
vs. DM+PRP+IgG								—	< **0.0001**	**0.0003**	**0.0004**
vs. DM+PRP+AntiVEGF-A Ab									—	< **0.0001**	< **0.0001**
vs. DM+VEGF-A 2										—	1
vs. DM+VEGF-A 20											—

Note. Differences were assessed by one-way ANOVA followed by Tukey's post hoc test. Statistical significance is shown in bold. All abbreviations are mentioned in the footnote to Table A1.

TABLE A7 *P*-Values resulting from the comparisons of instantaneous I_j values evoked at a given V_j from NIH/3T3 murine fibroblasts in the different conditions

V_j (mV)	DM+PRP+KRN633 vs. DM+PRP	DM+KRN633 vs. DM	DM+PRP+AntiVEGF-A Ab vs. DM+PRP	DM+VEGF-A 2 vs. DM+PRP
−150	0.175	0.430	0.427	0.807
−130	0.061	0.459	0.272	0.853
−110	**0.011**	0.562	0.151	0.937
−90	**0.002**	0.699	0.103	0.979
−70	< **0.0001**	0.651	0.083	0.888
−50	**0.0001**	0.822	0.088	0.767
−30	**0.0004**	0.666	0.091	0.630
−10	**0.001**	0.824	0.085	0.537
+10	**0.017**	**0.036**	0.103	0.916
+30	**0.017**	**0.011**	0.136	0.948
+50	**0.035**	**0.015**	0.210	0.995
+70	**0.017**	0.064	0.224	0.880
+90	0.074	**0.032**	0.370	0.913
+110	0.22	0.108	0.627	0.940
+130	0.702	0.272	0.950	0.880
+150	0.773	0.379	0.918	0.961

Note. Differences were assessed by Student's unpaired *t*-test. Statistical significance is shown in bold. All abbreviations are mentioned in the footnote to Table A1.

1469445x, 2022, 2, Downloaded from https://physoc.onlinelibrary.wiley.com/doi/10.1113/EP090052 by Universita Di Firenze Sistema, Wiley Online Library on [06/08/2024]. See the Terms and Conditions (https://onlinelibrary.wiley.com/terms-and-conditions) on Wiley Online Library for rules of use; OA articles are governed by the applicable Creative Commons License

TABLE A8 *P*-Values resulting from the comparisons of the steady-state I_j values evoked at a given V_j from NIH/3T3 murine fibroblasts in the different conditions

V_j (mV)	DM+PRP+KRN633 vs. DM+PRP	DM+KRN633 vs. DM	DM+PRP+AntiVEGF-A Ab vs. DM+PRP	DM+VEGF-A 2 vs. DM+PRP
−150	0.089	0.419	0.422	0.738
−130	**0.037**	0.465	0.334	0.708
−110	**0.001**	0.527	0.226	0.740
−90	**< 0.0001**	0.577	0.074	0.796
−70	**0.0002**	0.407	0.083	0.779
−50	**0.001**	0.553	0.087	0.836
−30	**0.001**	0.846	0.081	0.942
−10	**0.0003**	0.962	**0.048**	0.925
+10	**0.0002**	0.352	0.054	0.752
+30	**0.0002**	0.328	0.116	0.948
+50	**0.0005**	0.397	0.241	0.867
+70	**0.009**	0.436	0.445	0.867
+90	**0.046**	0.551	0.765	0.779
+110	0.145	0.655	0.859	0.809
+130	0.962	0.595	0.791	0.811
+150	0.976	0.562	0.668	0.732

Note. Differences were assessed by Student's unpaired *t*-test. Statistical significance is shown in bold. All abbreviations are mentioned in the footnote to Table A1.

TABLE A9 *P*-Values resulting from the comparisons of the $G_{j,ss}/G_{j,inst}$ ratios at a given V_j from NIH/3T3 murine fibroblasts in the indicated conditions

V_j (mV)	DM+PRP+KRN633 vs. DM+PRP	DM+KRN633 vs. DM	DM+PRP+AntiVEGF-A Ab vs. DM+PRP	DM+VEGF-A 2 vs. DM+PRP
−150	0.081	**0.034**	0.129	0.316
−130	0.067	0.209	0.126	0.357
−110	0.096	0.252	0.344	0.827
−90	0.756	0.205	0.735	0.525
−70	0.125	0.210	0.239	0.929
−50	0.061	0.180	0.261	0.869
−30	**0.011**	0.405	0.211	0.899
−10	**0.034**	0.979	**0.041**	0.129
+10	**0.002**	0.979	**0.033**	0.697
+30	0.618	0.948	**0.040**	0.850
+50	0.475	0.897	0.156	0.725
+70	0.953	0.782	0.456	0.553
+90	0.925	0.989	0.588	0.353
+110	0.888	0.998	0.559	0.325
+130	0.864	0.801	0.252	0.325
+150	0.934	0.684	0.283	0.354

Note. Differences were assessed by Student's unpaired *t*-test. Statistical significance is shown in bold. All abbreviations are mentioned in the footnote to Table A1.

1469445x, 2022, 2, Downloaded from https://physoc.onlinelibrary.wiley.com/doi/10.1113/EP090052 by Universita Di Firenze Sistema, Wiley Online Library on [06/08/2024]. See the Terms and Conditions (https://onlinelibrary.wiley.com/terms-and-conditions) on Wiley Online Library for rules of use; OA articles are governed by the applicable Creative Commons License